Journal of Alloys and Compounds 509 (2011) 4891–4895

Contents lists available at ScienceDirect

Journal of Alloys and Compounds

journal homepage: www.elsevier.com/locate/jallcom

# Microstructure and properties of the in situ formed amorphous-crystalline composites in the Fe–Cu-based immiscible alloys

Tomasz Kozieł[a,*], Anna Zielińska-Lipiec[a], Jerzy Latuch[b], Sławomir Kąc[a]

[a] AGH – University of Science and Technology, Faculty of Metals Engineering and Industrial Computer Science, Av. Mickiewicza 30, 30-059 Cracow, Poland
[b] Warsaw University of Technology, Faculty of Materials Science and Engineering, Wołoska Street 141, 02-507 Warsaw, Poland

ARTICLE INFO

*Article history:*
Received 7 July 2010
Received in revised form 19 January 2011
Accepted 30 January 2011
Available online 4 February 2011

*Keywords:*
Melt spinning
Metallic glasses
Liquid miscibility gap
TEM
Nanoindentation

ABSTRACT

The paper presents microstructures and mechanical properties of the melt-spun $Fe_{30}Cu_{32}Si_{13}B_9Al_8Ni_6Y_2$ and $Fe_{44}Cu_{18}Si_{13}B_9Al_8Ni_6Y_2$ alloys. It was found that liquid phase separation of the initially homogeneous melt occurred due to a positive heat of mixing between two major elements. The microstructures of the melt-spun ribbons were composed of the Fe-rich amorphous and the Cu-rich crystalline phases. A significant effect of the melt ejection temperature and the chemical composition (Fe and Cu content) on microstructures of rapidly solidified alloys was revealed. The microstructures of ribbons melt-spun from the miscibility gap region were non-uniform. On the other hand the microstructures of ribbons melt-spun from homogeneous melt temperature region were composed of the spherical precipitates distributed within the matrix. Superior hardness values of the examined ribbons melt-spun from the same temperature were found for the alloy with higher iron content. An increase of the melt-ejection temperature in the homogeneous melt region resulted in hardness decrease in case of the $Fe_{30}Cu_{32}Si_{13}B_9Al_8Ni_6Y_2$ alloy and its increase for the $Fe_{44}Cu_{18}Si_{13}B_9Al_8Ni_6Y_2$ ribbons.



## 1. Introduction

Amorphous metallic alloys offer attractive mechanical and physical properties due to lack of lattice defects, mainly dislocations. Metallic glasses, formed upon quenching of the melt at cooling rates high enough to hinder crystallization process, are easily obtained in a form of melt-spun ribbons or rods. Despite high strength of metallic glasses its application is still very limited because of low plasticity caused by highly localized shear banding [1,2]. In order to improve ductility of these materials, a composite microstructure, consisting of the crystalline phase dispersed in the amorphous matrix, is desired. Such microstructure can be obtained by in situ formation of a crystalline phase during cooling of the melt [3–7]. Final properties of composites are determined by morphology, volume fraction and distribution of reinforcing particles [8]. Based on the crack mechanics of polycrystalline materials, it is expected that spherical shape of precipitates would be desired. However during heterogeneous nucleation from a liquid state, precipitates tend to adopt dendrite shape.

Formation of spherical precipitates is possible in alloys with a liquid miscibility gap [9,10]. Such alloys, which are characterized by a positive heat of mixing between two major elements, decompose into two melts of different compositions. Because of lack of strain energy in the liquid state and relatively low surface energy between two melt, precipitates tend to adopt an ideal spherical shape. For sufficient glass forming ability (GFA) of an alloy, crystallization of both melts should be restrained and two-phase metallic glass could be formed. However positive heat of mixing between two basic elements, required for liquid/liquid phase separation, decreases GFA of alloys. Therefore two-phase metallic glasses reported so far were mainly formed by a melt spinning process [11–15]. In order to receive amorphous-crystalline composite structure, further vitrification of the amorphous phase with lower thermal stability is necessary.

Two coexisting melts have different chemical compositions and glass forming abilities. If GFA of one of the melt will be not sufficient, the amorphous-crystalline composite microstructure can be obtained during cooling [16–19]. This paper shows the microstructures and mechanical properties of the melt-spun $Fe_{30}Cu_{32}Si_{13}B_9Al_8Ni_6Y_2$ and $Fe_{44}Cu_{18}Si_{13}B_9Al_8Ni_6Y_2$ alloys. Two basic elements, i.e. iron and copper, exhibit positive heat of mixing as high as +13 kJ/mol [20], but the Fe–Cu phase diagram does not contain a liquid miscibility gap [21]. However Turchanin et al. [22] proved that undercooling of the homogeneous melt leads to decomposition into the Fe-rich and the Cu-rich melts. Selection of the alloying elements is explained in detail in Ref. [19].

In order to evaluate mechanical properties of the melt-spun ribbons, nanoindentation studies were carried out. It should be noted

* Corresponding author. Tel.: +48 12 617 26 21; fax: +48 12 617 31 90.
*E-mail address:* tkoziel@agh.edu.pl (T. Kozieł).

0925-8388/$ – see front matter © 2011 Elsevier B.V. All rights reserved.
doi:10.1016/j.jallcom.2011.01.203

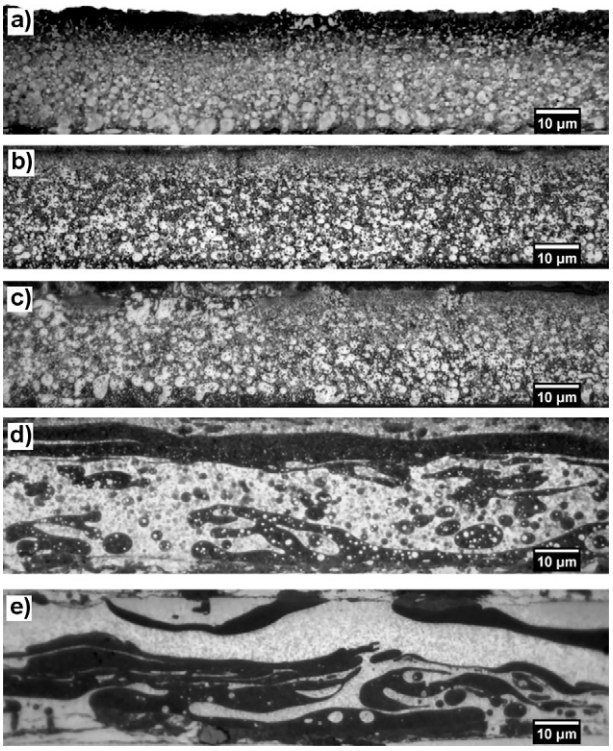


**Fig. 1.** LM microstructures of the $Fe_{30}Cu_{32}$ alloy melt-spun from: (a) 1520 °C; (b) 1450 °C; (c) 1400 °C; (d) 1330 °C; (e) 1230 °C (cross sections of the ribbons).

**Table 1**
Melt-ejection temperatures of the examined alloys.

| Alloy | Melt-ejection temperature, °C | | | | |
|---|---|---|---|---|---|
| $Fe_{30}Cu_{32}$ | 1230 | 1330 | 1400 | 1450 | 1520 |
| $Fe_{44}Cu_{18}$ | – | 1330 | 1400 | 1450 | 1520 |

however that hardness of thin ribbons should not be compared with results obtained for bulk materials.

## 2. Experimental

Two alloys, $Fe_{30}Cu_{32}$ and $Fe_{44}Cu_{18}$, with nominal composition of $Fe_{32}Cu_{32}Si_{13}B_9Al_8Ni_6Y_2$ and $Fe_{44}Cu_{18}Si_{13}B_9Al_8Ni_6Y_2$ (at.%), respectively, were prepared by arc melting of a mixture of high purity elements (99.9% or higher) under titanium gettered argon protective atmosphere. Rapidly solidified ribbons were prepared by single roller melt spinning facility (Edmund Bühler melt spinner HV) equipped with infrared radiation pyrometer under an argon atmosphere at a linear wheel speed of 40 m/s and a protective gas (argon) pressure of 50 kPa. In order to examine effect of the melt ejection temperature on the microstructure and properties of the ribbons, the alloys were melt-spun from different temperatures (Table 1). The lowest melt ejection temperature is typical for fabrication of a single-phase metallic glasses (about 50 °C above liquidus). Cross section of each ribbon was observed by means of light microscopy (LM). Moreover some ribbons were selected for scanning electron microscopy (SEM) studies using Zeiss FEG-SEM DSM982 Gemini microscope. Standard 3 mm discs were cut out from the ribbons and thinned by Gatan 691 ion polishing system. Thin foils were studied using JEOL JEM-200 CX transmission electron microscope (TEM), operating at 200 kV. Structures of the melt-spun ribbons were examined by X-ray diffraction (XRD) method (TuR M62 equipped with goniometer HZG4, Co-Kα radiation). Hardness ($H_{IT}$) of the ribbons was determined using CSM Nano-Hardness Tester equipped with Berkovich indenter at loading/unloading rates of 600 mN/min and a maximum load of 300 mN.

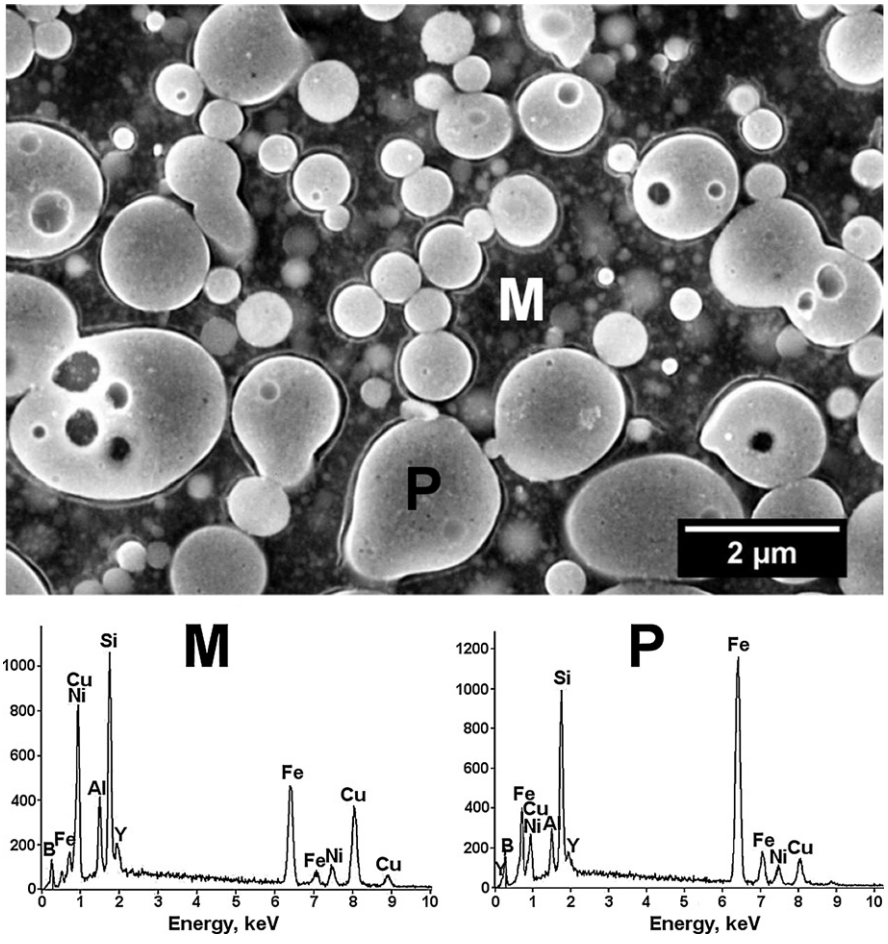


**Fig. 2.** SEM microstructure of the $Fe_{30}Cu_{32}$ alloy melt-spun from 1450 °C with EDS spectra of the matrix (M) and the precipitate (P).

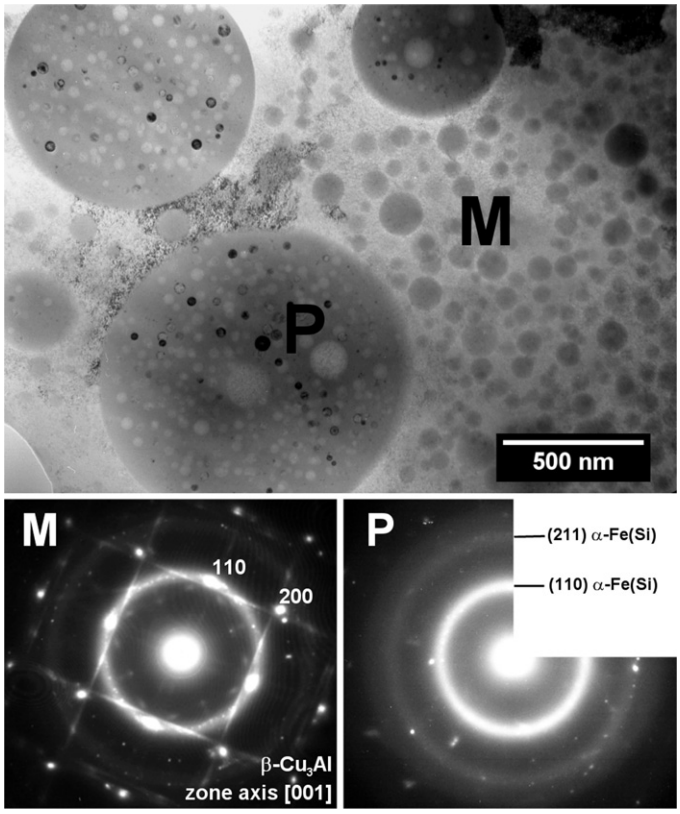


**Fig. 3.** TEM bright field image the $Fe_{30}Cu_{32}$ alloy melt-spun from 1400 °C with SAED patterns of the matrix (M) and the precipitate (P).

## 3. Results

The microstructures of the melt-spun $Fe_{30}Cu_{32}Si_{13}B_9Al_8Ni_6Y_2$ ($Fe_{30}Cu_{32}$) alloy, observed on the cross sections, are presented in Figs. 1 and 2. Coarse-segregated, non-uniform areas observed in the microstructure of ribbons melt-spun from 1230 and 1330 °C (Fig. 1d and e), indicate that the two melts, the Fe- and the Cu-rich, coexisted in the crucible prior to rapid cooling. On the other hand microstructures of the ribbons melt-spun from 1400, 1450 and 1520 °C (Fig. 1a–c) are composed of bright spherical precipitates distributed within a dark matrix. SEM observations of the ribbon melt-spun from 1450 °C supported by energy-dispersive spectroscopy (EDS) analysis, revealed that the matrix is composed of the Cu-rich phase whereas precipitates are enriched in iron (Fig. 2). Chemical compositions of the matrix and precipitates, locally determined by EDS, were $Fe_{11.0}Cu_{40.8}Si_{11.7}B_{21.7}Al_{7.7}Ni_{5.6}Y_{1.5}$ and $Fe_{46.0}Cu_{10.7}Si_{11.5}B_{23.2}Al_{3.1}Ni_{4.7}Y_{0.8}$ (at.%), respectively. TEM observations of the $Fe_{30}Cu_{32}$ alloy melt-spun from homogeneous melt temperature region (1400 °C) proved that the matrix is composed of the crystalline phase, whereas the primary formed spherical precipitates are amorphous (Fig. 3). SAED patterns of matrix (M) and precipitate (P) indicate at the presence of the crystalline bcc β-$Cu_3Al$ and the amorphous Fe-rich phases, respectively. However on the diffraction pattern obtained from matrix, a halo ring was also observed due to the presence of very fine amorphous precipitates. Moreover, some spots are visible in amorphous diffraction pattern resulting from precipitation of the secondary-formed crystalline Cu-rich phases.

The microstructure of the $Fe_{44}Cu_{18}Si_{13}B_9Al_8Ni_6Y_2$ ($Fe_{44}Cu_{18}$) ribbons observed by LM (Fig. 4) consists of a bright matrix and dark precipitates. SEM-EDS analysis of ribbon melt-spun from 1450 °C, confirmed that the matrix is composed of the Fe-rich matrix (Fig. 5) with composition of $Fe_{52.8}Cu_{7.9}Si_{12.3}B_{15.4}Al_{4.6}Ni_{6.1}Y_{0.9}$. Size of precipitates in the $Fe_{44}Cu_{18}$ alloy did not allow to estimate precisely its chemical composition. TEM bright field image of the ribbon melt-spun from 1520 °C (Fig. 6) proved that the matrix constituted the amorphous phase whereas the precipitates were formed from previously existing the Cu-rich melt. SAED pattern of precipitate (P) indicates at the formation of bcc β-$Cu_3Al$ phase. Size of the smallest crystalline particles observed in the amorphous matrix is far below 100 nm. Moreover in the primarily formed crystalline particles, some spherical amorphous precipitates were present.

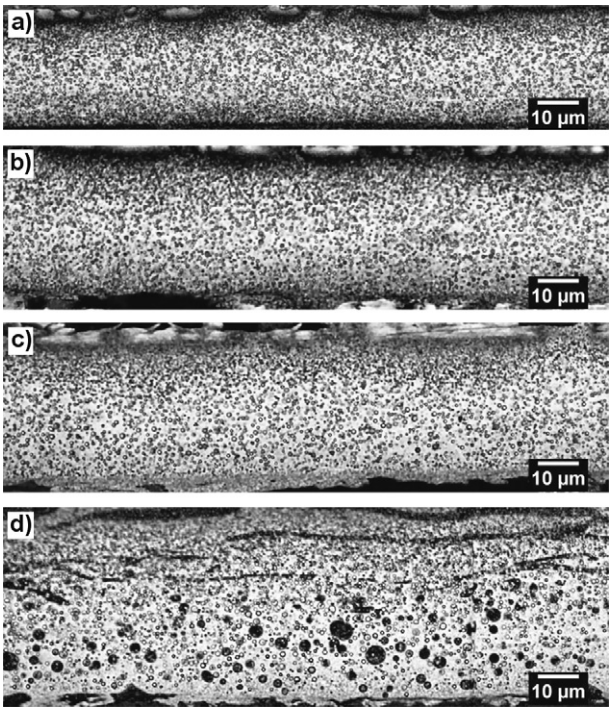


**Fig. 4.** LM microstructures of the $Fe_{44}Cu_{18}$ alloy melt-spun from: (a) 1520 °C; (b) 1450 °C; (c) 1400 °C; (d) 1330 °C (cross sections of the ribbons).

The structure of rapidly cooled alloys was examined by means of XRD (Fig. 7). Three crystalline phases, $Cu_3Al$, α-Fe(Si) and $Fe_2B$, were identified. Peaks with highest intensity corresponded to $Cu_3Al$ phase, observed by means of TEM.

Results of nanoindentation measurements are summarized in Table 2. For each melt-ejection temperature, hardness of the

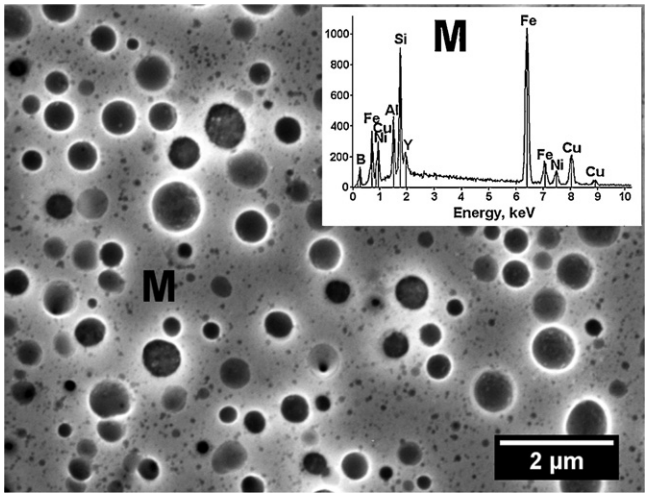


**Fig. 5.** SEM microstructure of the $Fe_{44}Cu_{18}$ alloy melt-spun from 1450 °C with EDS spectrum of the matrix (inset).

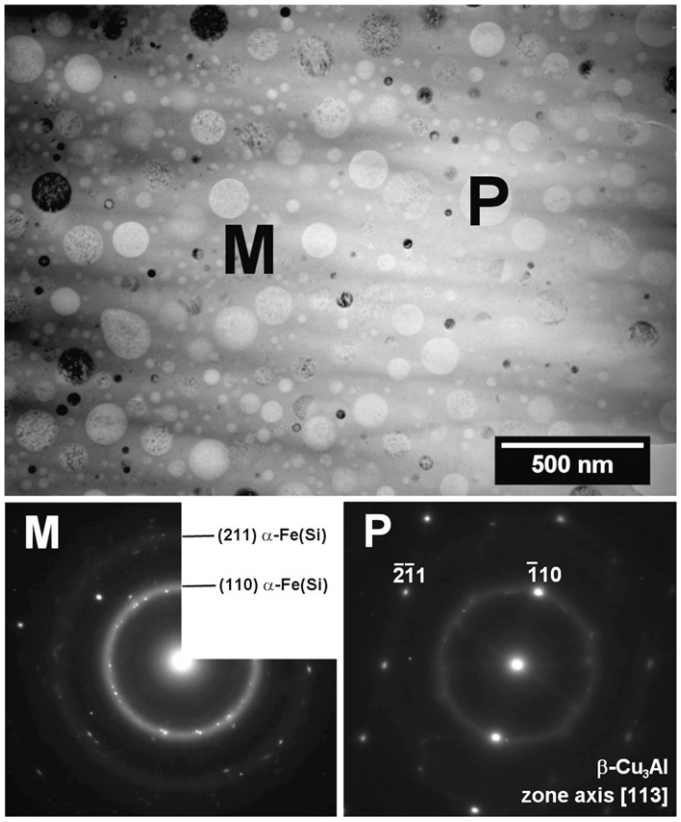


**Fig. 6.** TEM bright field image of the $Fe_{44}Cu_{18}$ alloy melt-spun from 1520 °C with SAED patterns of the matrix (M) and the precipitate (P).

**Table 2**
Results of nanoindentation studies of the examined ribbons.

| Alloy | Melt-ejection temperature, °C | Hardness $H_{IT}$, MPa |
|---|---|---|
| $Fe_{30}Cu_{32}$ | 1330 | 8717 ± 1652 |
| | 1400 | 7726 ± 427 |
| | 1450 | 7021 ± 267 |
| | 1520 | 6733 ± 657 |
| $Fe_{44}Cu_{18}$ | 1330 | 9275 ± 892 |
| | 1400 | 9737 ± 734 |
| | 1450 | 9293 ± 522 |
| | 1520 | 11,076 ± 400 |

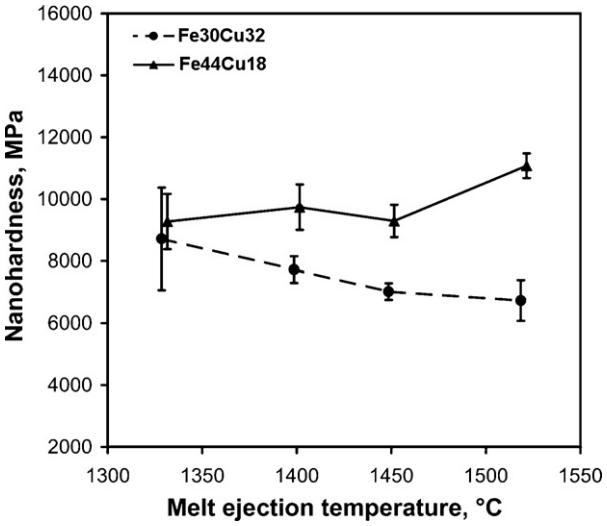


**Fig. 8.** Effect of the melt-ejection temperature on nanohardness of the examined melt-spun alloys.

$Fe_{44}Cu_{18}$ alloy was higher compared to the $Fe_{30}Cu_{32}$. Effect of the melt ejection temperature on hardness of both melt-spun alloys is presented in Fig. 8. Hardness of the $Fe_{30}Cu_{32}$ alloy decreased with increasing melt-ejection temperature, while increased for the $Fe_{44}Cu_{18}$ alloy.

## 4. Discussion

LM microstructures (Figs. 1 and 4) indicate at the importance of the melt-ejection temperature for alloys with the liquid miscibility gap. Based on microscopic observations of the melt-spun ribbons it is concluded that the critical temperatures for attaining homogeneous melt in both alloys are located between 1330 and 1400 °C. In order to obtain relatively uniform microstructure with spherical precipitates distributed within the matrix, alloys should be heated above the miscibility gap. When a homogeneous melt is cooled below a critical temperature, a driving force for decomposition appears, which induces precipitation process in a liquid state. Precipitates adopt a spherical shape which provides lowest surface energy. Further decrease in temperature reduces mutual solubility of two major elements. For sufficient undercooling, precipitation of the secondary-formed spheres proceeds in supersaturated primary-formed particles. Precipitation of spheres in spheres (fractal-like microstructure) is continued

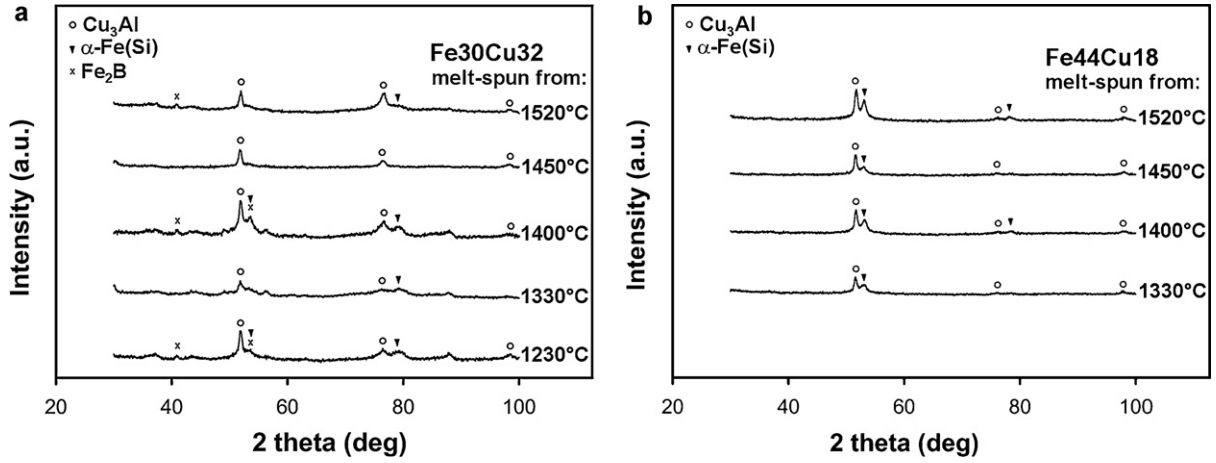


**Fig. 7.** XRD patterns of the (a) $Fe_{30}Cu_{32}$; (b) $Fe_{44}Cu_{18}$ melt-spun alloys (air side of the ribbons).

until glass-transition temperature or crystallization temperature is reached.

The microstructures of the $Fe_{30}Cu_{32}$ melt-spun ribbons were composed of the crystalline matrix and the amorphous precipitates, formed from previously existing Fe-rich (Fe, Si, B, Ni) and Cu-rich (Cu, Al, Ni, Y) melts, respectively. Partial substitution of copper with iron shifted chemical composition to the opposite site of the miscibility gap maximum. Thus in the $Fe_{44}Cu_{18}$ alloy, precipitation of the Cu-rich phase from the Fe-rich matrix occurred in a liquid state. In both alloys the Fe-rich melt became amorphous, when the glass transition temperature was reached. On the other hand, the Cu-rich liquid crystallized due to its lower glass forming ability. XRD and TEM studies revealed crystallization of the bcc $Cu_3Al$ phase. The presence of the crystalline α-Fe(Si) and $Fe_2B$ phases on XRD patterns (Fig. 7) is related with lower glass forming ability of the Fe-rich melt in a lower range of the miscibility gap. With a drop of temperature, which is a driving force for decomposition, the chemical composition and glass forming ability of both melts are changing.

Due to the mechanical properties of pure basic elements, hardness of the $Fe_{44}Cu_{18}$ melt-spun ribbons is higher compared to the $Fe_{30}Cu_{32}$. Estimation of volume fractions of precipitates was not possible, because its size vary from tens of microns to nanometres. It is assumed however, that different effects of the melt-ejection temperature on hardness of the melt-spun alloys results from decreasing volume fractions of precipitates. The increase of the melt-ejection temperature in the $Fe_{30}Cu_{32}$ alloy reduced volume fraction of the Fe-rich amorphous phase, leading to hardness decrease. In the case of the $Fe_{44}Cu_{18}$ alloy volume fraction of the softer Cu-rich precipitates decreases, leading to the highest hardness of the ribbon melt-spun from 1520 °C.

## 5. Conclusions

Rapid cooling made possible in situ formation of the amorphous-crystalline composites with a fractal-like microstructure. Microstructural observations of the $Fe_{30}Cu_{32}$ and $Fe_{44}Cu_{18}$ alloys revealed liquid/liquid phase separation into the Fe-rich and the Cu-rich melts. Ribbons should be cooled from a homogeneous melt temperature region in order to obtain microstructure composed of the spherical precipitates distributed within a matrix. Both melts may constitute either a matrix or precipitates, depending on chemical composition of the alloy. The Cu-rich melt crystallized as the bcc β-$Cu_3Al$ phase, whereas the Fe-rich melt became amorphous.

An increase of the melt ejection temperature in homogeneous melt region decreases volume fraction of precipitates formed upon cooling through the miscibility gap.

## Acknowledgments

The study was supported by Polish Ministry of Science and Higher Education under project No. 11.11.110.790.

## References

[1] W.L. Johnson, Mater. Sci. Forum 225/227 (1996) 35–50.
[2] Z.F. Zhang, J. Eckert, L. Schultz, Metall. Mater. Trans. A 35 (2004) 3489–3498.
[3] H. Tan, Y. Zhang, Y. Li, Intermetallics 10 (2002) 1203–1205.
[4] C. Fan, R.T. Ott, T.C. Huhnagel, Appl. Phys. Lett. 81 (2002) 1020–1022.
[5] H. Tan, Y. Zhang, X. Hu, Y. Li, Ann. Chim. Sci. Mater. 27 (2002) 119–124.
[6] X. Hu, S.C. Ng, Y.P. Feng, Y. Li, Acta Mater. 51 (2003) 561–572.
[7] M. Calin, J. Eckert, L. Schultz, Scripta Mater. 48 (2003) 653–658.
[8] A. Leonhard, L.Q. Xing, M. Heilmaier, A. Gebert, J. Eckert, L. Schultz, Nanostruct. Mater. 10 (1988) 805–817.
[9] A.A. Kündig, M. Ohnuma, D.H. Ping, T. Ohkubo, K. Hono, Acta Mater. 52 (2004) 2441–2448.
[10] T. Kozieł, Vitrification of alloys with a liquid miscibility gap. PhD thesis (in Polish). Kraków, 2009.
[11] B.J. Park, H.J. Chang, D.H. Kim, W.T. Kim, Phys. Rev. Lett. 96 (2006) 245503.
[12] B.J. Park, H.J. Chang, D.H. Kim, W.T. Kim, Appl. Phys. Lett. 85 (2004) 6353–6355.
[13] N. Mattern, U. Kühn, A. Gebert, T. Gemming, M. Zinkevich, H. Wendrock, L. Schultz, Scripta Mater. 53 (2005) 271–274.
[14] A.A. Kündig, M. Ohnuma, T. Ohkubo, T. Abe, K. Hono, Scripta Mater. 55 (2006) 449–452.
[15] E.S. Park, D.H. Kim, Acta Mater. 54 (2006) 2597–2604.
[16] T. Kozieł, Z. Kędzierski, A. Zielińska-Lipiec, J. Latuch, G. Cieslak, J. Microsc. 237 (2010) 267–270.
[17] K. Ziewiec, Z. Kędzierski, A. Zielińska-Lipiec, J. Stępiński, S. Kąc, J. Alloys Compd. 482 (2009) 114–117.
[18] K. Ziewiec, Z. Kędzierski, J. Alloys Compd. 480 (2009) 306–310.
[19] T. Kozieł, Z. Kędzierski, A. Zielińska-Lipiec, K. Ziewiec, Scripta Mater. 54 (2006) 1991–1995.
[20] F.R. de Boer, R. Boom, W.C.M. Mattens, A.R. Miedema, A.K. Niessen, Cohesion and Structure. Cohesion in Metals, vol. 1, Elsevier Science, Amsterdam, 1988.
[21] T.B. Massalski, H. Okamoto, P.R. Subramanian, L. Kacprzak, Binary Alloy Phase Diagrams, 2nd ed., AMS International, 1992.
[22] M.A. Turchanin, P.G. Agraval, I.V. Nikolaenko, J. Phase Equilib. 24 (2003) 307–319.